

## Article

# Gr/3D–ZnO Nanocomposites as Humidity Sensors with Enhanced Sensing Response

Wang-De Lin <sup>1,\*</sup>, You-Chen Lin <sup>2</sup>, Ren-Jang Wu <sup>2</sup> and Murthy Chavali <sup>3</sup> 

<sup>1</sup> Department of Center for General Education, St. Mary's Junior College of Medicine, Nursing and Management, Yilan 26647, Taiwan

<sup>2</sup> Department of Applied Chemistry, Providence University, Taichung 43301, Taiwan; lialisa3062988@gmail.com (Y.-C.L.); wurenjang@gmail.com (R.-J.W.)

<sup>3</sup> NTRC-MCETRC and Aarshanano Composite Technologies Pvt. Ltd., Guntur District, Medikonduru 522201, India; ChavaliM@gmail.com

\* Correspondence: newwander@smc.edu.tw

**Abstract:** This work introduces a novel humidity sensor based on a nanocomposite material comprising graphene decorated with three-dimensional flower-like structures of zinc oxide (Gr/3D–ZnO) fabricated via a hydrothermal method with various weight percentages of graphene. The surface structure and morphology of the Gr/3D–ZnO nanocomposite were analyzed using XRD, EDS, SEM, TEM, and Raman spectroscopy. The influence of humidity on the electrical properties of the nanocomposite was also investigated. Experiment results revealed that the nanocomposite with 70 wt% of graphene provided high sensitivity ( $S = 446$ ) with rapid response times (120 s) and recovery times (160 s). These results demonstrate the excellent potential of the proposed Gr/3D–ZnO nanocomposite in monitoring atmospheric humidity. A discussion on the mechanism underlying the effects of humidity on the Gr/3D–ZnO nanocomposite is also provided.

**Keywords:** graphene; ZnO; humidity sensor; nanocomposite



**Citation:** Lin, W.-D.; Lin, Y.-C.; Wu, R.-J.; Chavali, M. Gr/3D–ZnO Nanocomposites as Humidity Sensors with Enhanced Sensing Response. *Polymers* **2021**, *13*, 1623. <https://doi.org/10.3390/polym13101623>

Academic Editors: Shaowei Zhang and Tanveer A. Tabish

Received: 25 March 2021

Accepted: 11 May 2021

Published: 17 May 2021

**Publisher's Note:** MDPI stays neutral with regard to jurisdictional claims in published maps and institutional affiliations.



**Copyright:** © 2021 by the authors. Licensee MDPI, Basel, Switzerland. This article is an open access article distributed under the terms and conditions of the Creative Commons Attribution (CC BY) license (<https://creativecommons.org/licenses/by/4.0/>).

## 1. Introduction

Atmospheric levels of water vapor (i.e., humidity) can profoundly affect electronic devices, meteorological phenomena, agriculture, manufacturing, and food storage [1]. Efforts to control humidity levels depend on accurate measurements [2]; therefore, researchers are constantly striving to develop low-cost humidity sensors with ever-higher sensitivity and accuracy and ever-faster response and recovery times [3].

Numerous types of humidity sensors have been developed using resistive [4,5] and capacitive devices [6,7], quartz crystal microbalances [8–10], optical devices [11,12], and even surface acoustic waves [13,14]. This very particular research has also led to the development of materials and nanostructures that are highly sensitive to humidity, including TiO<sub>2</sub> nanopowders [15] and nanotubes [16], ZnO nanowires [17], WO<sub>3</sub> nanosheets [18], Fe<sub>2</sub>O<sub>3</sub> nanopowders [19], graphene layers [20], organic/inorganic polymers [21], ZrO<sub>2</sub> nanorods [22], and NiO–SnO<sub>2</sub> nanofibers [23]. Among the various metal oxides used for humidity sensing, n-type Zinc oxide (ZnO) semiconductors offer low cost, a high surface area ratio, high stability, and excellent chemical reactivity [24]. ZnO can be synthesized into various nanostructures, such as nanowires [25], nanorods [26], nanosheets [27], nanoparticles [28], nanofibers [29], hollow spheres [30], and nanoflowers [31]. Despite these successes, and because of the extremely exposed surface area, ZnO often suffers from self-aggregation, which may reduce the materials effective area to lower performance. Poor response in low humidity environments and large hysteresis limits the application of pure ZnO [32]. Nonetheless, sensing performance can be improved through the control of morphology and other modification methods, such as doping and the formation of compounds [33]. Graphene, a transparent single-layer two dimensional of sp<sup>2</sup> bonded

carbon atoms, has a large surface to volume ratio and excellent conductivity [34–36], which makes it very suitable for humidity sensing material. Humidity sensors based on graphene sensing layer have been developed by researchers and exhibit the advantage of high sensitivity and fast response recovery to different humidity [37–41]. The hydrophobic nature of pure graphene limits its applicability in humidity sensors; however, researchers have demonstrated the potential of decorating graphene with metal oxide nanoparticles to fabricate high-performance humidity sensors [42,43]. The incorporation of metal oxide within RGO sheets increases the number of active sites (e.g., vacancies and defects), which greatly enhances humidity sensing performance [44,45].

Our objective in this study was to fabricate a sensor based on a nanocomposite material comprising graphene decorated with three-dimensional flower-like structures of zinc oxide (Gr/3D-ZnO). The surface structure and morphology of the Gr/3D-ZnO nanocomposite were characterized using XRD, EDS, SEM, TEM, and Raman spectroscopy. We also investigated the influence of humidity on the electrical properties of the nanocomposite. The completed humidity sensor exhibited ultra-high sensitivity with fast recovery and response times over a broad range of relative humidity (RH) levels.

## 2. Experimental

### 2.1. Materials

Commercial graphene film of high purity (>99%) was purchased from UniRegion Bio-Tech (New Taipei City, Taiwan) and Sigma-Aldrich Co., Inc. (St. Louis, MO, USA). Zinc nitrate hexahydrate ( $\text{Zn}(\text{NO}_3)_2 \cdot 6\text{H}_2\text{O}$ , 98%), anhydrous alcohol ( $\text{C}_2\text{H}_5\text{OH}$ , 99.5%), L-histidine ( $\text{C}_6\text{H}_9\text{N}_3\text{O}_2$ ,  $\geq 99\%$ ), urea ( $(\text{NH}_2)_2\text{CO}$ , 99.5%), and polyvinyl alcohol (PVA, 99+% hydrolyzed) were purchased from Sigma-Aldrich Co., Inc.

### 2.2. Fabrication of Gr/3D-ZnO Nanocomposite Material

The 3D-ZnO structures prepared as per the methods outlined in [46]. Briefly, 100 mL of 0.1 M zinc nitrate hexahydrate ( $\text{Zn}(\text{NO}_3)_2 \cdot 6\text{H}_2\text{O}$ ) and 10 mL of 1 M urea were mixed for 5 min. To this solution was slowly added 20 mL of an aqueous solution containing 0.05 M of L-histidine while stirring roughly 15 min at room temperature (RT). The mixture was then transferred into a Teflon-lined autoclave for hydrothermal treatment at 120 °C for 4 h. The resulting precipitate was collected via centrifugation and washed using deionized water and ethanol before being dried under a vacuum at 80 °C. Finally, Gr/3D-ZnO was obtained via calcination at 400 °C for 2 h. Tests were performed on nanocomposite sensing materials fabricated using graphene in various ratios (10, 20, 30, 50, 70, and 80 wt%).

### 2.3. Characterization

The surface morphology and structure of the proposed Gr/3D-ZnO nanocomposite were examined using transmission electron microscopy and energy-dispersive X-ray spectroscopy (TEM/EDS; JEM-2100F). The crystal structure of Gr/3D-ZnO was characterized using an XRD-6000 Shimadzu X-ray diffractometer with  $\text{Cu K}\alpha$  radiation of 1.5405 Å at 40 kV and 30 mA between 10° and 80° (2 $\theta$ ) at intervals of 2°/min. Infrared spectra were measured using an Agilent Cary spectrophotometer. The characteristic Raman spectrum of the Gr/3D-ZnO nanocomposite was measured at RT under excitation from a laser source at a wavelength of 532 nm (Jobin Yvon iHR550, HORIBA).

### 2.4. Sensor Fabrication and Humidity Testing

A solution of 10% PVA was added to promote the binding of the composite. A pair of comb-like gold electrodes were applied to an alumina substrate via dip-coating (10 × 5 mm<sup>2</sup>), whereupon the chips were heated to 80 °C and held at that temperature for 0.5 h before undergoing calcination at 400 °C for 2 h.

The experiment setup used to assess the performance of the humidity sensor is described in our previous work [42]. Briefly, the sensitivity of the device to humidity was measured in a dynamic flow system with the sensors held in an airtight glass chamber

maintained at  $25\text{ }^{\circ}\text{C} \pm 2\text{ }^{\circ}\text{C}$  (Figure 1). Air was injected into the water to generate water vapour, which was subsequently pumped into the testing chamber. The specific RH was maintained at a given level for 15 min to enable the system to reach equilibrium. A thermo-hygrometer (Rotronic) with an accuracy of  $\pm 0.1\%$  was connected to the testing chamber to obtain ground-truth measurements of the RH within. This commercial humidity sensor was calibrated to a standard concentration at Center of Measurement Standards, Industrial Technology Research Institute, Chutung, Hsinchu, Taiwan 31040. The sensing response ( $S$ ) of the sensor to fluctuations in RH was defined as  $S = R_d/R_h$ , where  $R_d$  is the resistance of the sensor under dry conditions (12% RH) and  $R_h$  is the resistance under a specific level of humidity [43]. The humidity hysteresis properties were investigated by increasing the humidity from 12% to 90% and then decreasing it to 12% to facilitate the adsorption and desorption of water molecules.

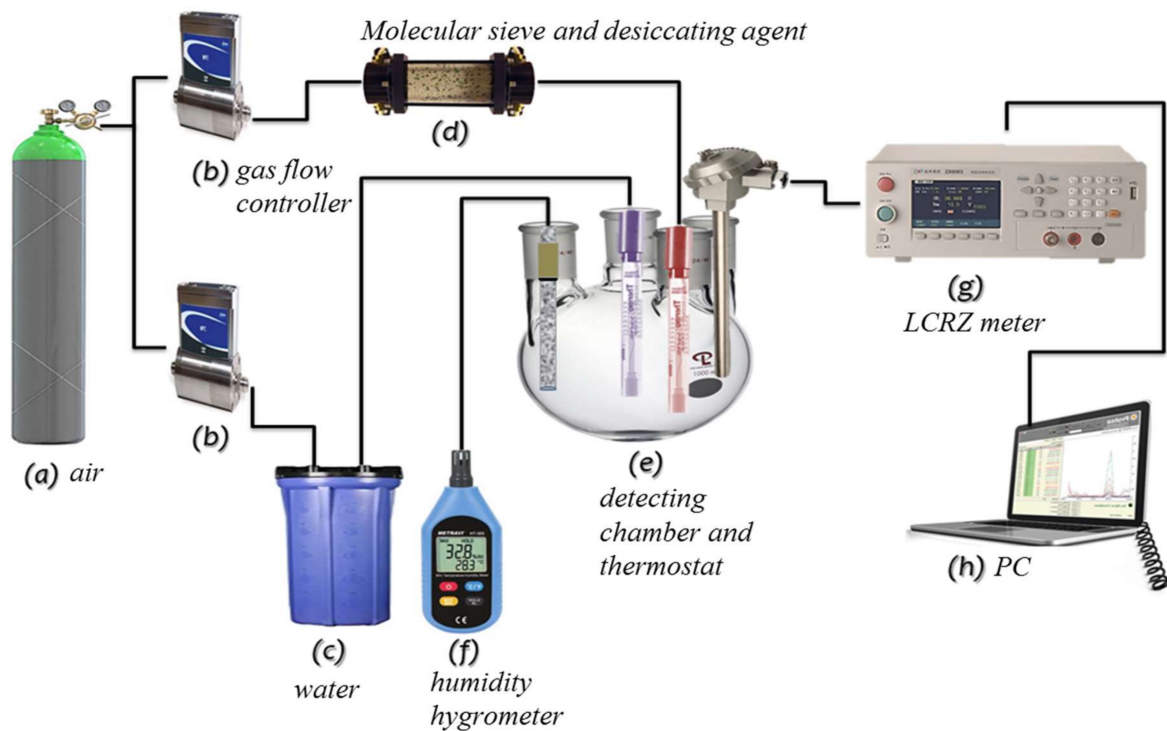


Figure 1. Experimental setup.

Humidity hysteresis error ( $H$ ) was calculated using the following equation:

$$H = \Delta f_{\max} / f_{fs} \times 100\%,$$

where  $\Delta f_{\max}$  indicates the maximum hysteresis error and  $f_{fs}$  indicates the full-scale response output [47]. The response and recovery times were defined as the time required for the impedance of the sensor to change by a value equal to 90% of the total impedance. Recovery time was defined as the time required for the process to be reversed [48]. RH was adjusted dynamically between 12% and 90% by altering the air:water ratio fed into the chamber. The impedance response of the sensing material to ambient humidity was measured using a chemical impedance analyzer (Delta United, DU 6010) with an input voltage of 1 V operating at a frequency of 1 kHz.

### 3. Results and Discussion

#### 3.1. Characterization of the Nanocomposite Structure

Figure 2 presents the XRD spectra of graphene, 3D-ZnO, and Gr/3D-ZnO with G concentrations of 10, 20, 30, 50, 70, and 80 wt%. As shown in Figure 2, XRD peaks indicative of graphene were observed at  $26.42^{\circ}$  [49]. The peaks at  $31.6^{\circ}$ ,  $34.2^{\circ}$ ,  $36.2^{\circ}$ ,  $47.5^{\circ}$ ,  $56.4^{\circ}$ ,

62.7°, 67.7°, and 72.2° (2 $\theta$  degrees), respectively corresponding to the (100), (002), (101), (102), (110), (103), (112) and (004) planes, similar to the typical hexagonal wurtzite structure of 3D-ZnO (JCPDS standard card No. 36-1451) [32]. Figure 2 present the spectra of five Gr/3D-ZnO samples, which revealed no new crystalline phases. Overall, these results demonstrate that the sensing material was a simple mixture.

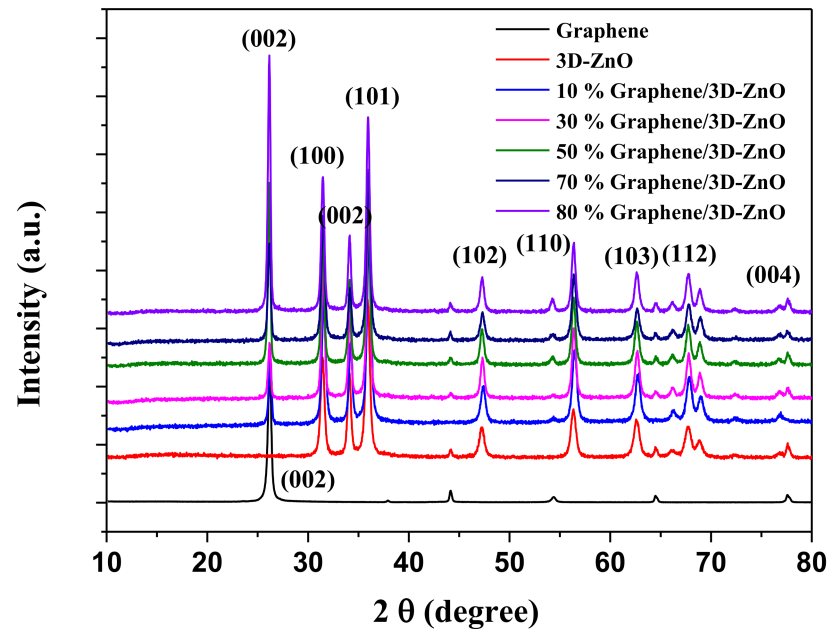


Figure 2. XRD analysis of Gr/3D-ZnO nanocomposite.

As shown in Figure 3, the crystalline structure of the samples was confirmed via Raman spectroscopy. Two prominent peaks indicative of defects in the D and G positions (at 1301  $\text{cm}^{-1}$  and 1568  $\text{cm}^{-1}$ ) were presumably due to in-plane bond stretching of  $\text{sp}^2$  hybridized carbon atoms and the corresponding combinational modes and overtones [50,51]. The peaks at 342 and 430  $\text{cm}^{-1}$  are the vibrational modes of ZnO [52]. The Gr/3D-ZnO nanocomposite did not present any peaks indicative of ZnO.

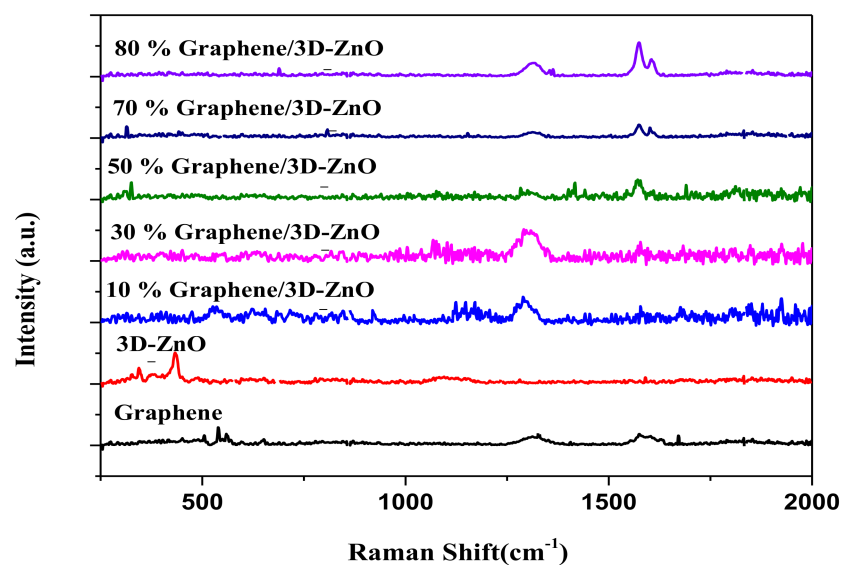
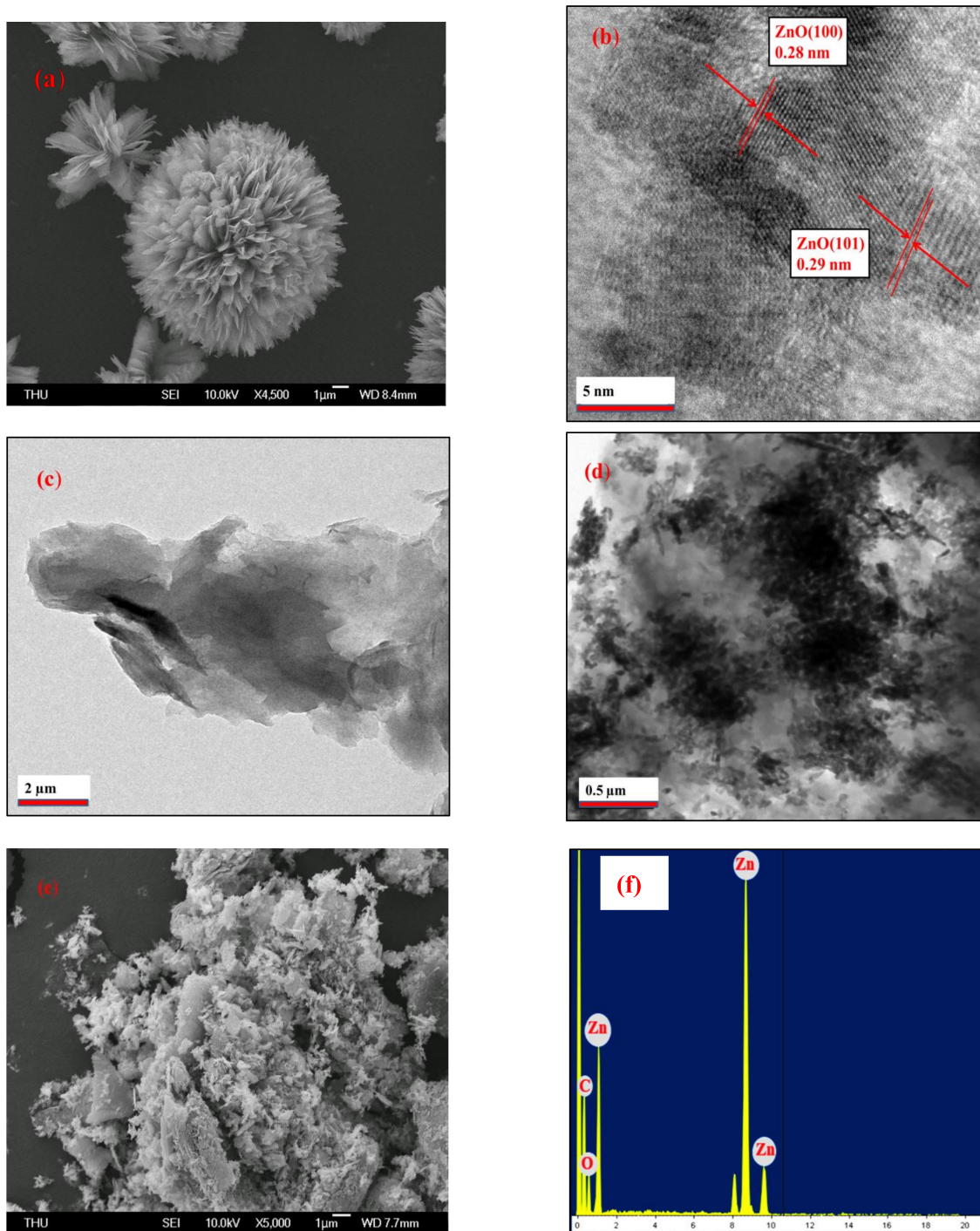


Figure 3. Raman spectra of Gr/3D-ZnO nanocomposite.

Figure 4 presents the SEM and TEM results used to characterize the morphology of the 3D-ZnO, graphene, and 70 wt% Gr/3D-ZnO nanocomposite. The SEM image in Figure 4a



illustrates the flower-like structure of 3D-ZnO. Figure 4b presents fringe spacing (0.28 nm and 0.29 nm) respectively indexed to the (100) and (101) planes of pure Wurtzite associated with the hexagonal structure of ZnO [53]. Figure 4c shows smooth graphene sheets stacked irregularly. Figure 4d,e reveals an abundance of 3D-ZnO aggregate on the surface of the 70 wt% Gr/3D-ZnO nanocomposite material. The EDS results in Figure 4f revealed peaks indicative of Zn, C, and O in the 70 wt% Gr/3D-ZnO nanocomposite. Overall, these results confirm the phase purity of the nanocomposite material.



**Figure 4.** (a) SEM image of 3D-ZnO flower-like structure, (b) TEM image of 3D-ZnO, (c) TEM image of graphene sheets, (d) TEM image of 70 wt% Gr/3D-ZnO, (e) SEM image of 70 wt% Gr/3D-ZnO nanocomposite, (f) EDX spectrum of 70 wt% Gr/3D-ZnO nanocomposite.

### 3.2. Sensitivity to Humidity

We assessed the sensitivity of Gr/3D-ZnO nanocomposite materials (Gr concentrations of 10, 20, 30, 50, 70, and 80 wt%) to humidity based on impedance measurements obtained using AC voltage (1V) at a frequency of 1 kHz. As shown in Figure 5a, the impedance of the sensor material decreased exponentially with an increase in the RH. As shown in Figure 5b, samples of 70 wt% Gr/3D-ZnO exhibited the highest sensitivity ( $S = 446$ ) across the range of humidity levels tested in this study (12–90%). We have selected 70 wt% Gr/3D-ZnO for all the subsequent analysis.

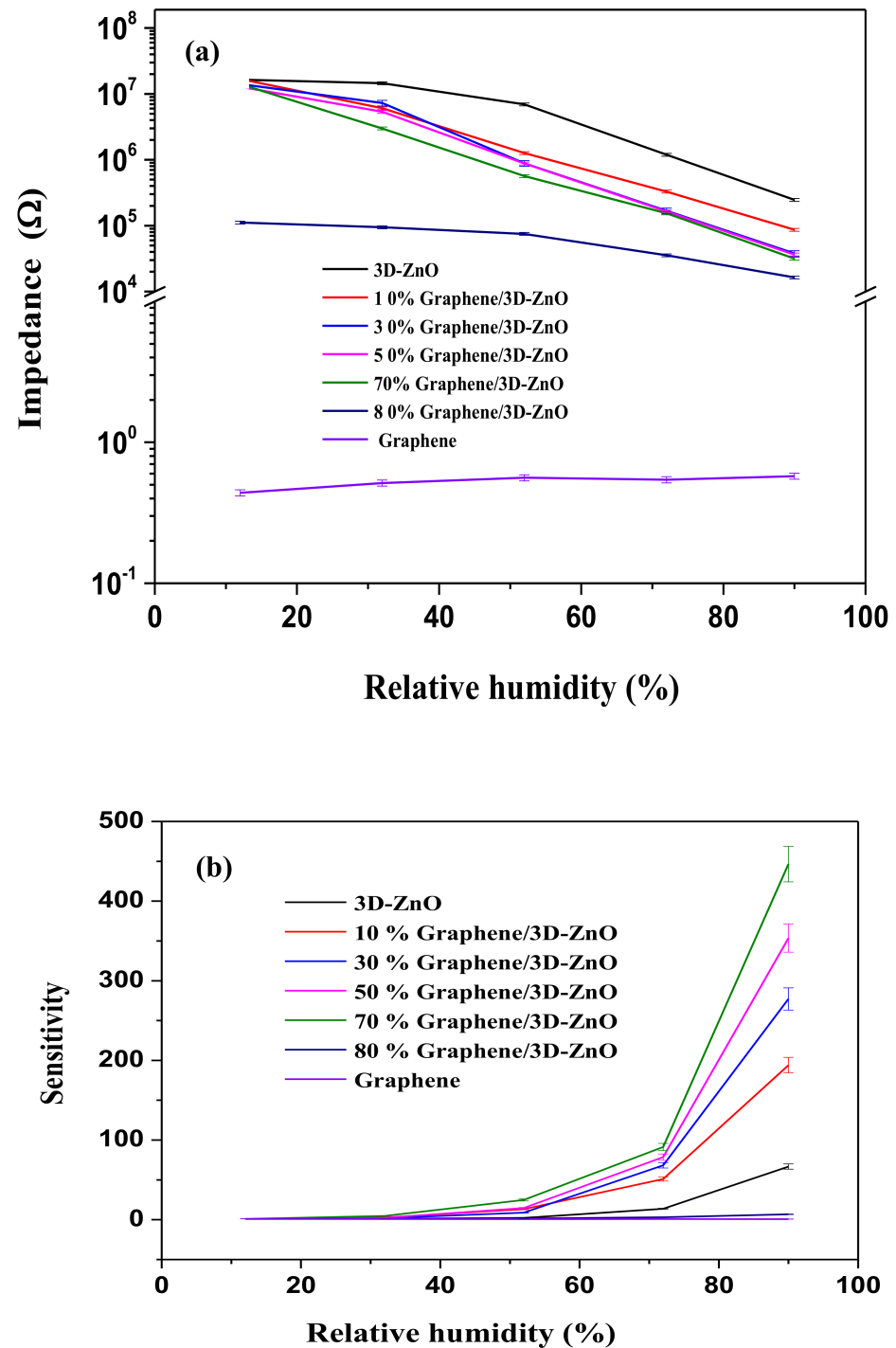
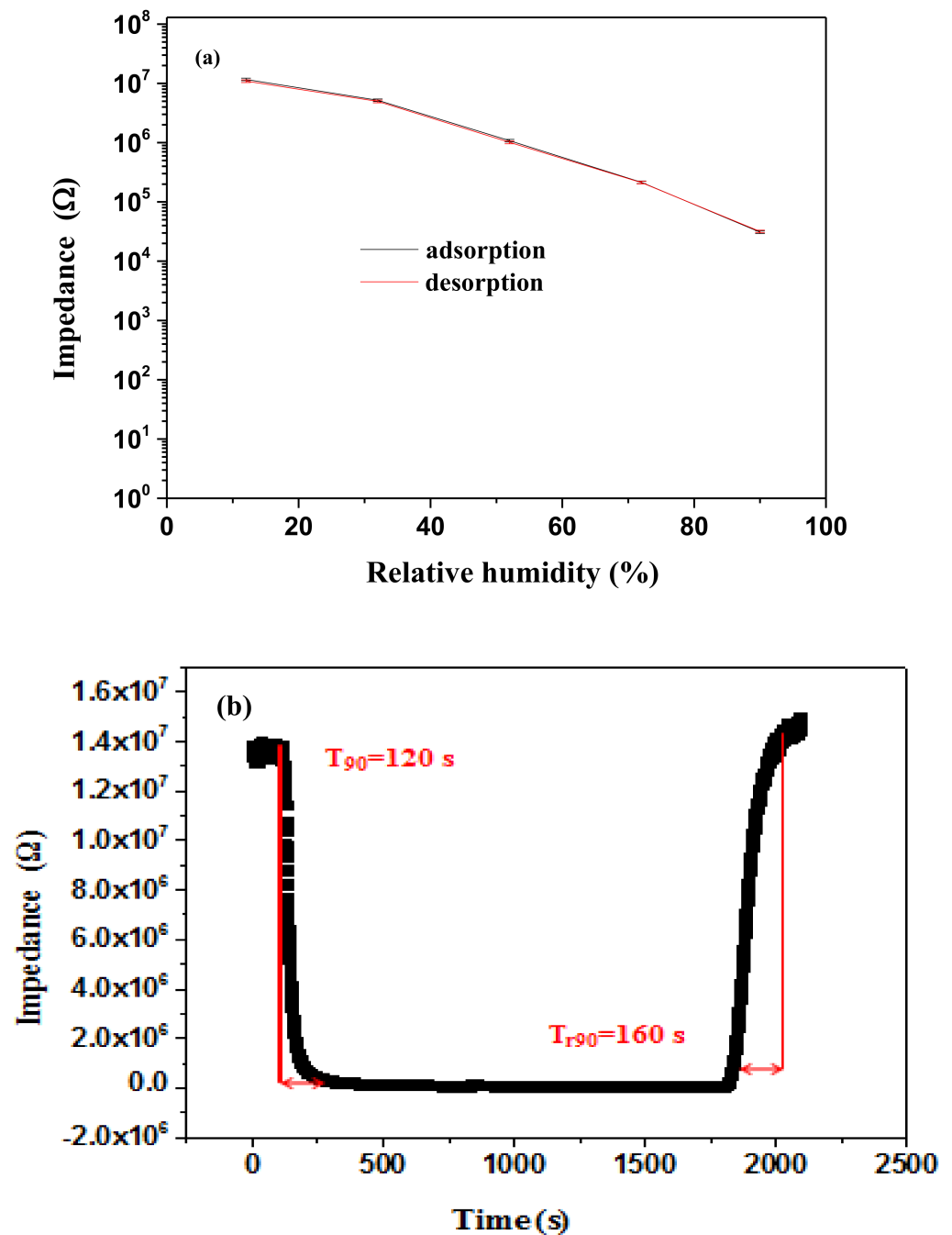


Figure 5. (a) Variation of impedance; (b) Variations in sensing response with the change in relative humidity (%) for different weight percentages of graphene in Gr/3D-ZnO nanocomposites.

Humidity hysteresis is an important factor in evaluating the reliability of humidity sensors [47]. As shown in Figure 6a, the 70 wt% Gr/3D–ZnO nanocomposite exhibited excellent reversibility, with nearly overlapping adsorption and desorption curves. The maximum hysteresis (2.32%) occurred under RH of 90%.



**Figure 6.** (a) Hysteresis characteristics (b) Response and recovery characteristics of 70 wt% Gr/3D–ZnO nanocomposites.

Response and recovery times largely determine the practical applicability of humidity sensors. As shown in Figure 6b, the impedance of 70 wt% Gr/3D–ZnO nanocomposite decreased rapidly with an increase in RH until reaching a relatively stable value (a total of 120 s). The impedance then returned rapidly to the original value in a very short time when humid air was replaced with dry air (a total of 160 s). Table 1 compares the proposed 70 wt% Gr/3D–ZnO sensor with previous works in terms of sensitivity, response times,

and recovery times [17,24,54–57]. Overall, the proposed Gr/3D–ZnO sensor performs well with all of the existing systems examined in this study.

**Table 1.** Comparison of humidity sensing ability of modified ZnO-based sensors that were previously reported.

Sensing Material	Measurement Range (% RH.)	Response Time (s)	Recovery Time (s)	References
ZnO nanowires	11–97	35.3	32.6	[17]
PVDF/ZnO nanocomposites	5–95	30	50	[24]
ZnO nanosheets	12–96	600	3	[54]
Sn-doped ZnO nanorod	40–90	230	30	[55]
LiCl-doped ZnO electrospun nanofibers	11–95	3	6	[56]
ZnO colloid crystals	5–98	152	10	[57]
Gr/3D–ZnO nanocomposites	12–90	120	160	This work

Selectivity is another crucial parameter in assessing the performance of humidity sensors. Figure 7 illustrates the selectivity of the 70 wt% Gr/3D–ZnO nanocomposite to an increase in humidity from 12% to 90% RH and various gases at concentrations of 1000 ppm under RT. The response of 70 wt% Gr/3D–ZnO nanocomposite to humidity was very high ( $R_{12\%}/R_{90\%} = 446$ ). The response to other gas species was as follows: CO (1.55), NH<sub>3</sub> (1.41), NO<sub>2</sub> (1.36), and NO (1.18). Overall, the Gr/3D–ZnO nanocomposite exhibited excellent selectivity for humidity.

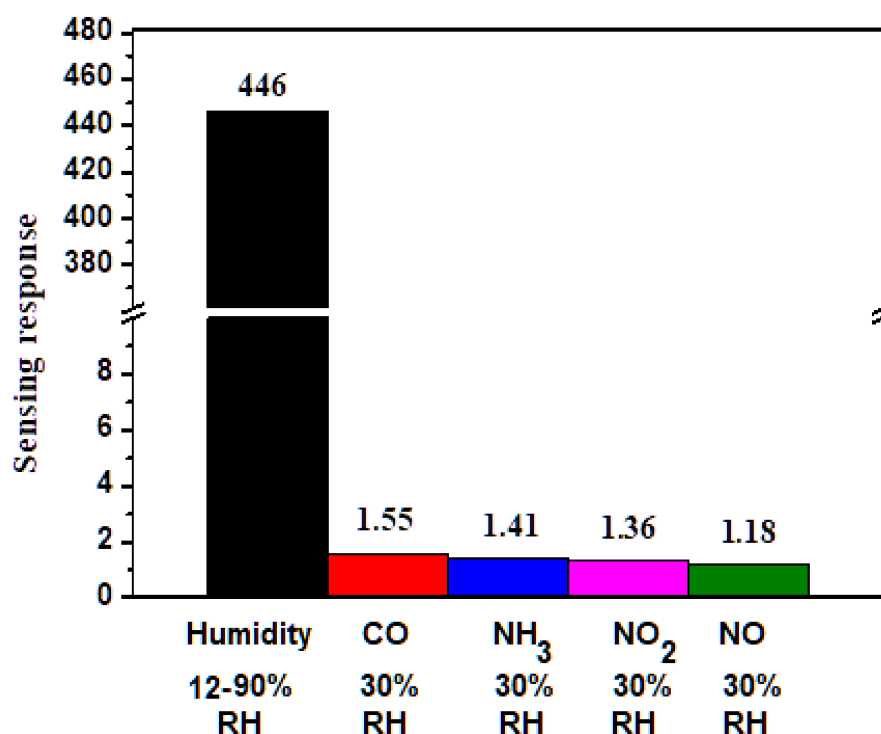


**Figure 7.** Selectivity for 70 wt% Gr/3D–ZnO nanocomposite towards humidity (12–90% RH), and gases like NO, NO<sub>2</sub>, NH<sub>3</sub>, CO (30% RH) at RT.

Figure 8 illustrates the stability of the prepared sensors as indicated by fluctuations in resistances under ambient RH of 12–90%. Only slight fluctuations in resistance were recorded over the 30-day testing period, regardless of the RH% environment.

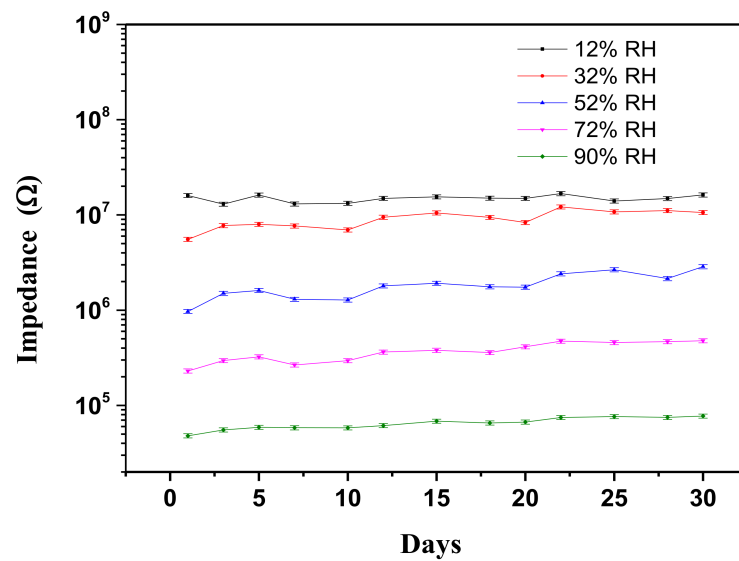


Figure 8. Long term stability of 70 wt% Gr/3D-ZnO nanocomposites at RT.

### 3.3. Sensing Mechanism

At low relative humidity (RH), the probability of contact between water molecules and Gr/3D-ZnO nanocomposite particles was low, so only the outer particles came into contact with the water molecules, as shown in Figure 9a. In this process, since water molecules could not form a continuous water layer, the transfer of  $\text{H}_2\text{O}$  or  $\text{H}_3\text{O}^+$  was on the discontinuous water layer was difficult [58]. Therefore, the Gr/3D-ZnO nanocomposite exhibited higher impedance at lower humidity. A relative high humidity (RH), one or several serial water layers were formed among the Gr/3D-ZnO nanocomposite particles, as presented in Figure 9b. The serial water layers accelerated the transfer of  $\text{H}_2\text{O}$  or  $\text{H}_3\text{O}^+$ . Grothuss and Casalbore-Miceli et al. outlined an ion transfer mechanism involving the transfer of  $\text{H}_2\text{O}$  or  $\text{H}_3\text{O}^+$  on serial water layers:  $\text{H}_2\text{O} + \text{H}_3\text{O}^+ \rightarrow \text{H}_3\text{O}^+ + \text{H}_2\text{O}$  [59,60]. This implies that the free movement of conduction ions increased the electrical conductivity of the Gr/3D-ZnO nanocomposite, which made it highly sensitive to humidity with quick response and recovery times.

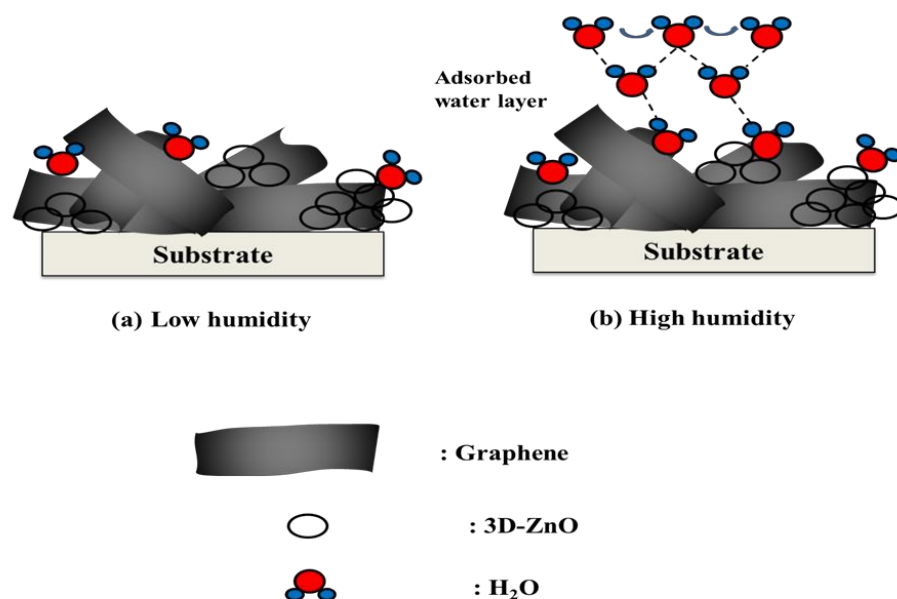


Figure 9. Scheme of humidity sensing mechanism (a) low humidity; (b) High humidity for Gr/3D-ZnO nanocomposite structure.



#### 4. Conclusions

In this work we have succeeded in fabricating Gr/3D-ZnO nanocomposites via a hydrothermal process to create a novel low-cost humidity sensor based on Gr/3D-ZnO nanocomposite material. Experiment results revealed that the nanocomposite with 70 wt% graphene provided a high sensitivity ( $S = 446$ ) with rapid response times (120 s) and recovery times (160 s). The highest humidity hysteresis error was only 2.32% over a wide range of RH values. These results demonstrate the excellent potential of the proposed Gr/3D-ZnO nanocomposite for the development of low-cost sensors to monitor atmospheric humidity.

**Author Contributions:** Conceptualization, W.-D.L., M.C.; methodology, W.-D.L., Y.-C.L.; software, W.-D.L., Y.-C.L.; validation, W.-D.L.; formal analysis, W.-D.L.; investigation, W.-D.L.; resources, R.-J.W.; data curation, W.-D.L., Y.-C.L.; writing—original draft preparation, W.-D.L.; writing—review and editing, W.-D.L., M.C.; visualization, R.-J.W. All authors have read and agreed to the published version of the manuscript.

**Funding:** This research received no external funding.

**Institutional Review Board Statement:** Not applicable.

**Informed Consent Statement:** Not applicable.

**Conflicts of Interest:** The authors declare that they have no known competing financial interests or personal relationships that could have appeared to influence the work reported in this paper.

#### References

1. Lee, C.-Y.; Lee, G.-B. Humidity sensors: A review. *Sens. Lett.* **2005**, *3*, 1–15. [[CrossRef](#)]
2. Blank, T.A.; Eksperiandova, L.P.; Belikov, K.N. Recent trends of ceramic humidity sensors development: A review. *Sens. Actuators B Chem.* **2016**, *228*, 416–442. [[CrossRef](#)]
3. Divya, T.; Nikhila, M.P.; Anju, M.; Arsha Kusumam, T.V.; Akhila, A.K.; Ravikiran, Y.T.; Renuka, N.K. Nanoceria based thin films as efficient humidity sensors. *Sens. Actuators A Phys.* **2017**, *261*, 85–93. [[CrossRef](#)]
4. Meng, W.; Wu, S.; Wang, X.; Zhang, D. High-sensitivity resistive humidity sensor based on graphitic carbon nitride nanosheets and their application. *Sens. Actuators B Chem.* **2020**, *315*, 128058. [[CrossRef](#)]
5. Ruiz, V.; Fernández, I.; Carrasco, P.; Cabañero, G.; Grande, H.J.; Herrán, J. Graphene quantum dots as a novel sensing material for low-cost resistive and fast-response humidity sensors. *Sens. Actuators B Chem.* **2015**, *218*, 73–77. [[CrossRef](#)]
6. Mallick, S.; Ahmad, Z.; Qadir, K.W.; Rehman, A.; Shakoor, R.A.; Touati, F.; Al-Muhtaseb, S.A. Effect of BaTiO<sub>3</sub> on the sensing properties of PVDF composite-based capacitive humidity sensors. *Ceram. Int.* **2020**, *46*, 2949–2953. [[CrossRef](#)]
7. Qi, R.; Zhang, T.; Guan, X.; Dai, J.; Liu, S.; Zhao, H.; Fei, T. Capacitive humidity sensors based on mesoporous silica and poly(3,4-ethylene dioxothiophene) composites. *J. Colloid Interface Sci.* **2020**, *308*, 127693.
8. Qi, P.; Xu, Z.; Zhang, T.; Fei, T.; Wang, R. Chitosan wrapped multiwalled carbon nanotubes as quartz crystal microbalance sensing material for humidity detection. *J. Colloid Interface Sci.* **2020**, *560*, 284–292. [[CrossRef](#)] [[PubMed](#)]
9. Qi, P.; Zhang, T.; Shao, J.; Yang, B.; Fei, T.; Wang, R. A QCM humidity sensor constructed by graphene quantum dots and chitosan composites. *Sens. Actuators A Phys.* **2019**, *287*, 93–101. [[CrossRef](#)]
10. Sun, Y.L.; Chen, Y.Z.; Wu, R.J.; Chavali, M.; Huang, Y.C.; Su, P.G.; Lin, C.C. Poly(l-lactide) stabilized gold nanoparticles based QCM sensor for low humidity detection. *Sens. Actuators B Chem.* **2007**, *126*, 441–446. [[CrossRef](#)]
11. Ascorbe, J.; Corres, J.M.; Matias, I.R.; Arregui, F.J. High sensitivity humidity sensor based on cladding-etched optical fiber and lossy mode resonances. *Sens. Actuators B Chem.* **2016**, *233*, 7–16. [[CrossRef](#)]
12. Yuan, T.; Qi, X.; Liu, Z.; Yang, J.; Guan, C.; Long, Q.; Cao, J.; Luo, M.; Yang, X.; Yuan, L. Humidity sensor based on micro-optical fiber array fabricated by electrospinning. *Opt. Commun.* **2018**, *427*, 517–521. [[CrossRef](#)]
13. Kuznetsova, I.E.; Anisimkin, V.I.; Kolesov, V.V.; Kashin, V.V.; Osipenko, V.A.; Gubin, S.P.; Tkachev, S.V.; Verona, E.; Sun, S.; Kuznetsova, A.S. Sezawa wave acoustic humidity sensor based on graphene oxide sensitive film with enhanced sensitivity. *Sens. Actuators B Chem.* **2018**, *272*, 236–242. [[CrossRef](#)]
14. Tang, Y.; Li, Z.; Ma, J.; Wang, L.; Yang, J.; Du, B.; Yu, Q.; Zu, X. Highly sensitive surface acoustic wave (SAW) humidity sensors based on sol-gel SiO<sub>2</sub> films: Investigations on the sensing property and mechanism. *Sens. Actuators B Chem.* **2015**, *215*, 283–291. [[CrossRef](#)]
15. Wu, R.J.; Sun, Y.L.; Lin, C.C.; Chen, H.W.; Chavali, M. Composite of TiO<sub>2</sub> nanowires and nafion as a humidity sensor material. *Sens. Actuators B Chem.* **2006**, *115*, 198–204. [[CrossRef](#)]
16. Liang, F.; Luo, L.-B.; Tsang, C.-K.; Zheng, L.; Cheng, H.; Li, Y.Y. TiO<sub>2</sub> nanotube-based field-effect transistors and their application as humidity sensors. *Mater. Res. Bull.* **2012**, *47*, 54–58. [[CrossRef](#)]

17. Park, S.; Lee, D.; Kwak, B.; Lee, H.-S.; Lee, S.; Yoo, B. Synthesis of self-bridged ZnO nanowires and their humidity sensing properties. *Sens. Actuators B Chem.* **2018**, *268*, 293–298. [[CrossRef](#)]
18. Parthibavarman, M.; Karthik, M.; Prabhakaran, S. Facile and one-step synthesis of WO<sub>3</sub> nanorods and nanosheets as an efficient photocatalyst and humidity sensing material. *Vacuum* **2018**, *155*, 224–232. [[CrossRef](#)]
19. Adhyapak, P.V.; Kadam, V.; Mahadik, U.; Amalnerkar, D.P.; Mulla, I.S. Influence of Li doping on the humidity response of maghemite ( $\gamma$ -Fe<sub>2</sub>O<sub>3</sub>) nanopowders synthesized at room temperature. *Ceram. Int.* **2013**, *39*, 8153–8158. [[CrossRef](#)]
20. Li, Z.-Y.; Yang, W.-J.; Wu, Y.-P.; Wu, S.-B.; Cai, Z.-B. Role of humidity in reducing the friction of graphene layers on textured surfaces. *Appl. Surf. Sci.* **2017**, *403*, 362–370. [[CrossRef](#)]
21. Liou, H.J.; Suyambrakasam, G.; Tsai, T.C.; Wu, R.J.; Chavali, M. Preparation of nanostructured organic/inorganic polymer hybrids and their humidity sensing properties. *J. Taiwan Inst. Chem. Eng.* **2011**, *42*, 868–873. [[CrossRef](#)]
22. Wang, Z.; Lu, Y.; Yuan, S.; Shi, L.; Zhao, Y.; Zhang, M.; Deng, W. Hydrothermal synthesis and humidity sensing properties of size-controlled Zirconium Oxide (ZrO<sub>2</sub>) nanorods. *J. Colloid Interface Sci.* **2013**, *396*, 9–15. [[CrossRef](#)] [[PubMed](#)]
23. Pascariu, P.; Airinei, A.; Olaru, N.; Petrilă, I.; Nica, V.; Sacarescu, L.; Tudorache, F. Microstructure, electrical and humidity sensor properties of electrospun NiO–SnO<sub>2</sub> nanofibers. *Sens. Actuators B Chem.* **2016**, *222*, 1024–1031. [[CrossRef](#)]
24. Arularasu, M.V.; Harb, M.; Vignesh, R.; Rajendran, T.V.; Sundaram, R. PVDF/ZnO hybrid nanocomposite applied as a resistive humidity sensor. *Surf. Interfaces* **2020**, *21*, 100780. [[CrossRef](#)]
25. Hsu, C.-L.; Chang, L.-F.; Hsueh, T.-J. Light-activated humidity and gas sensing by ZnO nanowires grown on LED at room temperature. *Sens. Actuators B Chem.* **2017**, *249*, 265. [[CrossRef](#)]
26. Dwiputra, M.A.; Fadhila, F.; Imawan, C.; Fauzia, V. The enhanced performance of capacitive-type humidity sensors based on ZnO nanorods/WS<sub>2</sub> nanosheets heterostructure. *Sens. Actuators B Chem.* **2020**, *310*, 127810. [[CrossRef](#)]
27. Modaresinezhad, E.; Darbar, S. Realization of a room-temperature/self-powered humidity sensor, based on ZnO nanosheets. *Sens. Actuators B Chem.* **2016**, *237*, 358–366. [[CrossRef](#)]
28. Niarchos, G.; Dubourg, G.; Afroudakis, G.; Tsouti, V.; Makarona, E.; Matović, J.; Crnojević-Bengin, V.; Tsamis, C. Paper-based Humidity Sensor Coated with ZnO Nanoparticles: The Influence of ZnO. *Procedia Eng.* **2016**, *168*, 325. [[CrossRef](#)]
29. Lin, Q.; Li, Y.; Yang, M. Investigations on the sensing mechanism of humidity sensors based on electrospun polymer nanofibers. *Sens. Actuators B Chem.* **2012**, *171–172*, 309–314. [[CrossRef](#)]
30. Perfecto, T.M.; Zito, C.A.; Volanti, D.P. Effect of NiS nanosheets on the butanone sensing performance of ZnO hollow spheres under humidity conditions. *Sens. Actuators B Chem.* **2021**, *334*, 129684. [[CrossRef](#)]
31. Zhu, D.; Ma, H.; Zhen, Q.; Xin, J.; Tan, L.; Zhang, C.; Wang, X.; Xiao, B. Hierarchical flower-like zinc oxide nanosheets in-situ growth on three-dimensional ferrocene-functionalized graphene framework for sensitive determination of epinephrine and its oxidation derivative. *Appl. Surf. Sci.* **2020**, *526*, 146721. [[CrossRef](#)]
32. Feng, M.H.; Wang, W.C.; Li, X.J. Capacitive humidity sensing properties of CdS/ZnO sesame-seedcandy structure grown on silicon nanoporous pillar array. *J. Alloys Compd.* **2017**, *698*, 94–98. [[CrossRef](#)]
33. Zhang, H.; Yu, S.; Chen, C.; Zhang, J.; Liu, J.; Li, P. Effects on structure, surface oxygen defects and humidity performance of Au modified ZnO via hydrothermal method. *Appl. Surf. Sci.* **2019**, *486*, 482–489. [[CrossRef](#)]
34. Yin, P.T.; Kim, T.-H.; Choi, J.-W.; Lee, K.-B. Prospects for graphene-nanoparticle-based hybrid sensors. *Phys. Chem. Chem. Phys.* **2013**, *15*, 12785. [[CrossRef](#)]
35. Latif, U.; Dickert, F. Graphene hybrid materials in gas sensing applications. *Sensors* **2015**, *15*, 30504–30524. [[CrossRef](#)]
36. Son, Y.J.; Chun, K.Y.; Kim, J.S.; Lee, J.H.; Han, C.S. Effects of chemical and physical defects on the humidity sensitivity of graphene surface. *Chem. Phys. Lett.* **2017**, *689*, 206–211. [[CrossRef](#)]
37. Lin, C.-H.; Chen, W.-T.; Huang, C.-H.; Woon, W.-Y.; Lin, C.-T. Effects of  $\pi$ -electron in humidity sensing of artificially stacked graphene bilayers modified with carboxyl and hydroxyl groups. *Sens. Actuators B Chem.* **2019**, *301*, 127020. [[CrossRef](#)]
38. Su, Y.; Li, C.; Li, M.; Li, H.; Xu, S.; Qian, L.; Yang, B. Surface acoustic wave humidity sensor based on three-dimensional architecture graphene/PVA/SiO<sub>2</sub> and its application for respiration monitoring. *Sens. Actuators B Chem.* **2020**, *308*, 127693. [[CrossRef](#)]
39. Ali, S.; Hassan, A.; Hassan, G.; Bae, J.; Lee, C.H. All-printed humidity sensor based on graphene/methyl-red composite with high sensitivity. *Carbon* **2016**, *105*, 23–32. [[CrossRef](#)]
40. Kilic, B.; Turkdogan, S. Fabrication of dye-sensitized solar cells using graphene sandwiched 3D–ZnO nanostructures based photoanode and Pt-free pyrite counter electrode. *Mater. Lett.* **2017**, *193*, 195. [[CrossRef](#)]
41. Huang, Y.; Chen, X.; Zhang, K.; Feng, X. Preparation of graphene supported flower-like porous 3D ZnO–NiO ternary composites for high capacity anode materials for Li-ion batteries. *Ceram. Int.* **2015**, *41*, 13532. [[CrossRef](#)]
42. Lin, W.-D.; Chang, H.-M.; Wu, R.-J. Humidity sensing properties of ZnO colloid crystals coated on quartz crystal microbalance by the self-assembly method. *Ceram. Int.* **2013**, *181*, 326–331.
43. Lin, W.-D.; Liao, C.-T.; Chang, T.-C.; Chen, S.-H.; Wu, R.-J. Humidity sensing properties of novel graphene/TiO<sub>2</sub> composites by sol-gel process. *Sens. Actuators B Chem.* **2015**, *209*, 555–561. [[CrossRef](#)]
44. Zhang, D.; Chang, H.; Li, P.; Liu, R.; Xue, Q. Fabrication and characterization of an ultrasensitive humidity sensor based on metal oxide/graphene hybrid nanocomposite. *Sens. Actuators B Chem.* **2016**, *225*, 233–240. [[CrossRef](#)]
45. Jlassi, K.; Mallick, S.; Eribi, A.; Chehimi, M.M.; Ahmad, Z.; Touati, F.; Krupa, I. Facile preparation of N-S co-doped graphene quantum dots (GQDs) from graphite waste for efficient humidity sensing. *Sens. Actuators B Chem.* **2021**, *328*, 129058. [[CrossRef](#)]

46. Basnet, P.; Chatterjee, S. Structure-directing property and growth mechanism induced by capping agents in nanostructured ZnO during hydrothermal synthesis—A systematic review. *Nano-Struct. Nano-Objects* **2020**, *22*, 100426. [[CrossRef](#)]
47. Yu, S.; Zhang, H.; Chen, C.; Lin, C. Investigation of humidity sensor based on Au modified ZnO nanosheets via hydrothermal method and first principle. *Sens. Actuators B Chem.* **2019**, *287*, 526–534. [[CrossRef](#)]
48. Gu, L.; Zheng, K.; Zhou, Y.; Li, J.; Mo, X.; Patzke, G.R.; Chen, G. Humidity sensors based on ZnO/TiO<sub>2</sub> core/shell nanorod arrays with enhanced sensitivity. *Sens. Actuators B Chem.* **2011**, *159*, 1–7. [[CrossRef](#)]
49. Shao, S.; Kim, H.W.; Kim, S.S.; Chen, Y.; Lai, M. NGQDs modified nanoporous TiO<sub>2</sub>/graphene foam nanocomposite for excellent sensing response to formaldehyde at high relative humidity. *Appl. Surf. Sci.* **2020**, *516*, 145932. [[CrossRef](#)]
50. Li, Y.; Deng, C.; Yang, M. Facilely prepared composites of polyelectrolytes and graphene as the sensing materials for the detection of very low humidity. *Sens. Actuators B Chem.* **2014**, *194*, 51–58. [[CrossRef](#)]
51. Zhang, L.; Zhang, J.; Huang, Y.; Xu, H.; Zhang, X.; Lu, H.; Xu, K.; Chu, P.K.; Ma, F. Hexagonal ZnO nanoplates/graphene composites with excellent sensing performance to NO<sub>2</sub> at room temperature. *Appl. Surf. Sci.* **2021**, *537*, 147785. [[CrossRef](#)]
52. Kumar, P.; Som, S.; Pandey, M.K.; Das, S.; Chanda, A.; Singh, J. Investigations on optical properties of ZnO decorated graphene oxide (ZnO@GO) and reduced graphene oxide (ZnO@r-GO). *J. Alloys Compd.* **2018**, *744*, 64–74. [[CrossRef](#)]
53. Nakrela, A.; Benramdane, N.; Bouzidi, A.; Kebbab, Z.; Medles, M.; Mathieu, C. Site location of Al-dopant in ZnO lattice by exploiting the structural and optical characterisation of ZnO:Al thin films. *Results Phys.* **2016**, *6*, 133–138. [[CrossRef](#)]
54. Tsai, F.-S.; Wang, S.-J. Enhanced sensing performance of relative humidity sensors using laterally grown ZnO nanosheets. *Sens. Actuators B Chem.* **2014**, *193*, 280–287. [[CrossRef](#)]
55. Ismail, A.S.; Mamat, M.H.; Md. Sin, N.D.; Malek, M.F.; Zoolfakar, A.S.; Suriani, A.B.; Mohamed, A.; Ahmad, M.K.; Rusop, M. Fabrication of hierarchical Sn-doped ZnO nanorod arrays through sonicated sol–Gel immersion for room temperature, resistive-type humidity sensor applications. *Ceram. Int.* **2016**, *42*, 9785–9795. [[CrossRef](#)]
56. Wang, W.; Li, Z.; Liu, L.; Zhang, H.; Zheng, W.; Wang, Y.; Huang, H.; Wang, Z.; Wang, C. Humidity sensor based on LiCl-doped ZnO electrospun nanofibers. *Sens. Actuators B Chem.* **2009**, *141*, 404–409. [[CrossRef](#)]
57. Yuan, Z.; Tai, H.; Bao, X.; Liu, C.; Ye, Z.; Jiang, Y. Enhanced humidity-sensing properties of novel graphene oxide/zinc oxide nanoparticles layered thin film QCM sensor. *Mater. Lett.* **2016**, *174*, 28–31. [[CrossRef](#)]
58. Anderson, J.H.; Parks, G.A. Electrical conductivity of silica gel in the presence of adsorbed water. *J. Phys. Chem.* **1968**, *72*, 3662. [[CrossRef](#)]
59. Agmon, N. The Grotthuss mechanism. *Chem. Phys. Lett.* **1995**, *244*, 456–462. [[CrossRef](#)]
60. Casalbore-Miceli, G.; Yang, M.J.; Camaioni, N.; Mari, C.M.; Li, Y.; Sun, H.; Ling, M. Investigations on the ion transport mechanism in conducting polymer films. *Solid State Ion.* **2000**, *131*, 311–321. [[CrossRef](#)]